Electronic Supplementary Information

Contents

1. DNA Sequences

The DNA strands for the walker and tracks of this study are indicated and marked in Fig. S1. The nucleotide sequence for each strand is given below the figure.

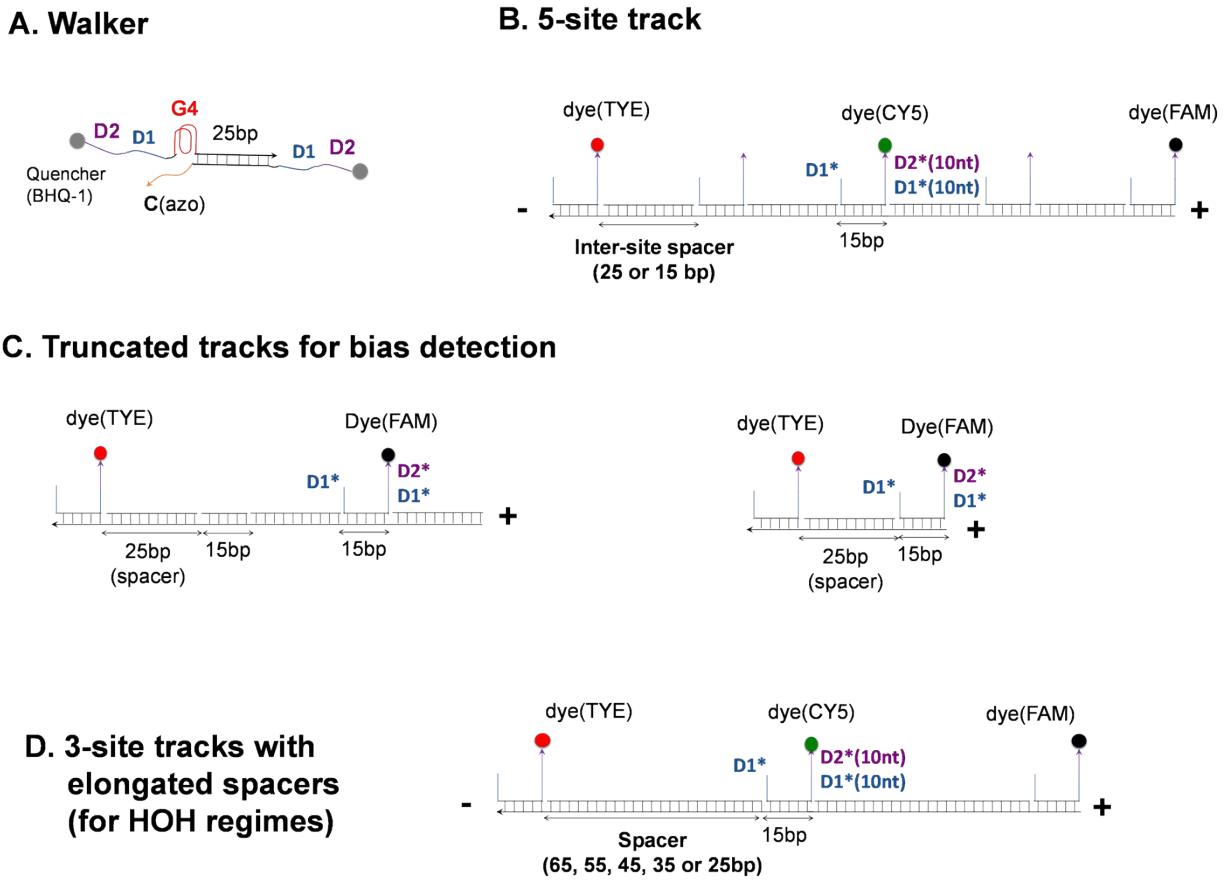

Figure S1. The motor and tracks used in this study. The constituent DNA strands are shown as continuous lines with key segments highlighted in different colors (red for G-quadruplex; yellow for the complementary azo-containing segment; purple and blue for legs and the binding partners on track).

DNA sequences (from 5' to 3' end; asterisk marks complementary sequences)

(A)Walker

The walker is made of two strands (see Figure S1, panel A)

G quadruplex-containing strand = BHQ-1-D2-D1-Linker-G4-B0;
Azo-containing strand = BHQ-1-D2-D1-Linker-B0*-C(azo).

The constituent segments have the following sequences:
D1 = TGGAATGACT; D2 = GTGATTGTAG;
Linker = ACCT; B0 = TATCTCCAGATTCATCGACGGCGGC;
G4 = GGGTTAGGGTTAGGGTTAGGG;
C(azo) = CXCCXTAXACXCCXTAXACXCCXTAXACXCC (X for azo-moieties).

(B)Tracks

The 5-site track (Figure S1, panel B)

It is made of five site strands, four identical spacer strands, and a template strand.
The site strands are
Site 1 = D1*-B1-D1*-D2*-FAM; Site 2 = D1*-B2-D1*-D2*;
Site 3 = D1*-B3-D1*-D2*-CY5; Site 4 = D1*-B4-D1*-D2*;
Site 5 = D1*-B5-D1*-D2*-TYE,
with
B1 = AGCGATTACTTGTGC; B2 = GTTCTTACCGCATGA
B3 = ACCACATTCTCCGGC; B4 = TTGAAGTCCGACCAT
B5 = CAACAGCAATGTTCG

Spacer strand (25mer): SP25 = GTGACTGCTCAAACACGGAGTAGCC
Spacer strand (15mer): SP15 = AAACACGGAGTAGCC

Template strand for the 5-site track with 25bp spacer:
TP25 = B1*-SP25*-B2*-SP25*-B3*-SP25*-B4*-SP25*-B5*
Template strand for the 5-site track with 15bp spacer:
TP15 = B1*-SP15*-B2*-SP15*-B3*-SP15*-B4*-SP15*-B5*

Mutated spacer: SP25(mutated) = GTTAGCGACGGATTTTGAGCCCCAG
(underlines mark native nucleotides)

The truncated tracks (Figure S1, panel C)

The track illustrated on panel C left is made of site 1, site 5, two spacer strands (SP25), a 15nt-long cover strand (B3), and a template as TP25(truncated1) = B1*-SP25*-B3*-SP25*-B5*.

The track illustrated on panel C right is made of site 1, site 5, one spacer strand (SP25), and a template as TP25(truncated2) = B1*-SP25*-B5*

The 3-site tracks with elongated spacers (Figure S1, panel D)

The tracks are each made of a template, two identical spacer strands (SPN), and three site strands (site 1, site 3 and site 5, with B3 segment in site 3 replaced by a new 15nt-long sequence as B3N = TTACAATCCGTCGTG).

The template strand is TPN = B1*-SPN*-B3N*-SPN*-B5*.
The spacer strands are
SPN(65mer) =
AGAGGCTCCGAGCTAGTCCAAGGGGATCGTAGTATTTTGCATGACAAAGCCC
CAGCCATTATAGC
SPN(55mer) =
AGCTAGTCCAAGGGGATCGTAGTATTTTGCATGACAAAGCCCCAGCCATTAT
AGC
SPN(45mer) =
AGCTAGTCCAAGGGGATCGTAGTATTTTGCATGACAAAGCCCCAG
SPN(35mer) = GTTAGGTAGTCGACGGTATTTTGAAGAAGCCCCAG
SPN(25mer) = GTTAGCGACGGATTTTGAGCCCCAG
SPN(15mer) = GTTAGCGACGCGAGG

(C) The separate C-fuel strand and Guanine-rich strand used to test the walker
(both sequences taken from ref.[1])

C-Fuel = CCCTAACACTAACGCTAAGCCTAACGT
Guanine-rich strand = ACGTTAGGATTAGCGTTAGTGTTA

2. Kinetic Model

Consider a bi-length nanowalker like the present one that matches two nearest binding sites in a contracted configuration under UV and matches three sites in an extended configuration under visible light. Further consider a 5-site track for the walker's operation. There are seven possible two-leg-bound states along the 5-site track, of which three are long states (over three sites) and four are short states (over two sites) (see schematic illustration of the seven states in Fig. S2, panel A). The UV induces transitions from a long state to two nearby short states by a branch ratio α_{uv}, and the visible light induces transitions from a short state to two nearby long states by another branch ratio α_{vis}.

Considering the site overlap, complete dissociation of a leg off track and the resultant single-leg-bound state are neglected at all sites except for those at the track's ends. This amounts to an approximation for ideal inchworm motion, whose characteristics will provide a reference to analyse the experiments of this study. However, the inchworm motion naturally results in leg dissociation and transient single-leg states at the track's two ends. As a consequence, flip-flop transitions occur from a two-leg state at the track's ends to another state in the middle, as schematically illustrated in panels B, C of Figure S2.

The operation of the inchworm walker on the 5-site track can be described by a Master Equation, which quantifies how the operation-induced transitions change the occupation probability of the walker on the seven states,

$$\frac{dP(t)}{dt} = M_{vis|uv} P(t). \qquad (1)$$

Here M_{vis} or M_{uv} applies depending on whether visible or UV illumination is being applied respectively. $P(t)$ is the state vector at time t, i.e., the occupation probabilities for the seven states.

$$P = \begin{pmatrix} p_1 \\ p_2 \\ p_3 \\ p_4 \\ p_5 \\ p_6 \\ p_7 \end{pmatrix}. \quad (2)$$

For a 1:1 walker-track ratio (equivalent of the equimolar walker-track mix used in this study), the state vector satisfies the normalization, i.e., $\sum_{i=1}^{7} p_i = 1$.

The transition matrix for each round of UV or visible light (M_{uv}, M_{vis}) can be expressed in terms of branch ratios associated with the transitions (shown in panel A of Figure S2).

$$M_{uv} = \frac{k_{uv}}{1+\alpha_{uv}} \times \begin{pmatrix} 0 & 1 & 0 & 0 & 0 & 0 & 0 \\ 0 & -1-\alpha_{uv} & 0 & 0 & 0 & 0 & 0 \\ 0 & \alpha_{uv} & 0 & 1 & 0 & 0 & 0 \\ 0 & 0 & 0 & -1-\alpha_{uv} & 0 & 0 & 0 \\ 0 & 0 & 0 & \alpha_{uv} & 0 & 1 & 0 \\ 0 & 0 & 0 & 0 & 0 & -1-\alpha_{uv} & 0 \\ 0 & 0 & 0 & 0 & 0 & \alpha_{uv} & 0 \end{pmatrix}. \quad (3)$$

$$M_{vis} = \frac{k_{vis}}{1+\alpha_{vis}} \times \begin{pmatrix} -1-\alpha_{vis} & 0 & 0 & 0 & 0 & 0 & 0 \\ 1 & 0 & \alpha_{vis} & 0 & 0 & 0 & 0 \\ 0 & 0 & -1-\alpha_{vis} & 0 & 0 & 0 & 0 \\ \alpha_{vis} & 0 & 1 & 0 & \alpha_{vis} & 0 & 1 \\ 0 & 0 & 0 & 0 & -1-\alpha_{vis} & 0 & 0 \\ 0 & 0 & 0 & 0 & 1 & 0 & \alpha_{vis} \\ 0 & 0 & 0 & 0 & 0 & 0 & -1-\alpha_{vis} \end{pmatrix}. \quad (4)$$

Here k_{uv} and k_{vis} are the rates for the transitions induced by UV and visible light.

The time-dependent solution of the Master Equation is $P(t) = \exp[tM_{vis}M_{uv}]P(t=0)$. If $P(N)$ is the state vector at the start of one round of light operation (i.e., UV followed by visible light), the state vector at the start of the next round is then $P(N+1) = \exp(\Delta t_{vis} M_{vis}) \exp(\Delta t_{uv} M_{uv}) P(N)$. Here Δt_{uv}, Δt_{vis} are the time duration

of the UV and visible light per round of operation. Introducing dimensionless durations $\Delta t^*_{uv} = \frac{k_{uv}\Delta t_{uv}}{1+\alpha_{uv}}$, $\Delta t^*_{vis} = \frac{k_{vis}\Delta t_{vis}}{1+\alpha_{vis}}$, the evolution of state vector is simplified as

$$P(N+1) = \exp(\Delta t^*_{\rm vis}\, M^*_{\rm vis}) \exp(\Delta t^*_{\rm uv}\, M^*_{\rm uv}) P(N), \quad (5)$$

where $M^*_{\rm vis}$ and $M^*_{\rm uv}$ are unitless transition matrices with $M^*_{\rm vis} = (1+\alpha_{\rm vis})M_{\rm vis}/k_{\rm vis}$ and $M^*_{\rm uv} = (1+\alpha_{\rm uv})M_{\rm uv}/k_{\rm uv}$.

Thus, we have a kinetic model for 5-site-supported inchworm motion with only four parameters: two dimensionless durations $\Delta t^*_{\rm uv}$, $\Delta t^*_{\rm vis}$, and two branch ratios $\alpha_{\rm uv}$, $\alpha_{\rm vis}$. Equivalently, the kinetic model can be specified by the two branch ratios plus another two parameters, $n_{\rm uv} = \Delta t^*_{\rm uv}(1+\alpha_{\rm uv}) = k_{\rm uv}\Delta t_{\rm uv}$, and $n_{\rm vis} = \Delta t^*_{\rm vis}(1+\alpha_{\rm vis}) = k_{\rm vis}\Delta t_{\rm vis}$, which are the probabilities of actual transitions per round of UV or visible light.

After N rounds of operation, the occupation probability changes as $\Delta p_-(N) = p_1(N) + p_2(N) - p_1(0) - p_2(0)$ for at the track's minus end, as $\Delta p_+(N) = p_6(N) + p_7(N) - p_6(0) - p_7(0)$ for the plus end. The initial occupation probabilities for the short states 1, 7 are $p_1(0) \sim 0$, $p_7(0) \sim 0$ since the walker and track are under the visible light before operation. Considering the identical nucleotide sequence for binding sites, the initial probabilities for the long states 2, 6 are $p_2(0) \sim 1/3$, $p_6(0) \sim 1/3$, equivalent of ~ 66% control-calibrated fluorescence at time zero, which is compatible with experimental values obtained from the pre-incubated equimolar walker-track mix (~ 62% for minus end and 75% for plus end, see Figure S4). Further consider the ~ 100% effective contact quenching ensured by the dye-quencher labeling scheme in this study, the change of control-calibrated fluorescence at the minus or plus ends follows the probabilities as $\Delta I_-(N) = -\Delta p_-(N)$; $\Delta I_+(N) = -\Delta p_+(N)$, yielding the γ value after N rounds of operation

$$\gamma = \frac{p_6(N) + p_7(N) - p_1(N) - p_2(N)}{\frac{1}{3} - p_1(N) - p_2(N)}. \quad (6)$$

Fig. S3 shows typical γ values versus operational cycles predicted for different parameters relevant to the present DNA walker. The figure also shows the predicted change of control-calibrated fluorescence (following $\Delta I_-(N) = -\Delta p_-(N)$; $\Delta I_+(N) = -\Delta p_+(N)$ for the minus and plus ends, and $\Delta I_{\rm m}(N) = -\Delta p_{\rm m}(N)$ for the middle site with the associated occupation change $\Delta p_{\rm m}(N) = p_2(N) + p_6(N) - p_2(0) - p_6(0)$).

The walker's asymptotic performance on the 5-site track after many operation rounds is reflected by the steady-state solution to the Master Equation (eq. 1), namely $P(\infty) = \exp(\Delta t^*_{\rm vis}\, M^*_{\rm vis}) \exp(\Delta t^*_{\rm uv}\, M^*_{\rm uv}) P(\infty)$. The steady-state state vector $P(\infty)$ is thus the eigenvector of the combined transition matrix $M_{\rm tot} = \exp(\Delta t^*_{\rm vis}\, M^*_{\rm vis}) \exp(\Delta t^*_{\rm uv}\, M^*_{\rm uv})$ with zero eigenvalue. Note that $\exp(M^*_{\rm vis} + M^*_{\rm uv}) \neq \exp(M^*_{\rm vis}) \exp(M^*_{\rm uv})$ since $M^*_{\rm vis}$ and $M^*_{\rm uv}$ do not commute.

The steady-state solution indicates that γ is capped by 1.5 for an inchworm walker on the 5-site track, as shown by exhaustive scanning of all four parameters of the kinetic model (Figure S4, panel A). The time-dependent solutions shown in Fig. S3 are all below

this limit. This upper limit is due to the flip-flop transitions at the track's ends, and the upper limit goes up to 3 without the transitions (panel B, Figure S3).

The upper limits have an intuitive interpretation. For an ideally effective inchworm walker operated on the 5-site track, the minus end is ultimately vacated (i.e., the asymptotic occupation probability $p_1(\infty) \sim 0$, $p_2(\infty) \sim 0$). But the walker is unable to accumulate at the plus end due to the flip-flop transition: it sends the walker from the ending state 6 backward to the middle state 4 through UV-dependent transient state 7, while the inchworm motion continues to send the walker forward from state 4 to state 6 (see panel B, Figure S2). As a consequence, the walker is cycled between two long states (4 and 6), both of which are stable under visible light, sharing the walker population equally for an ideally effective inchworm motion. Hence $p_6(\infty) \sim 50\%$ as measured under the visible light, while $p_7(\infty) \sim 0$ due to instability of state 7 under the visible light. These asymptotic probabilities yield the γ upper limit of 1.5 by eq. 6. Without the flip-flop transitions, the walker may accumulate in state 6 at the plus end by ~ 100%, yielding the γ upper limit of 3 by eq. 6.

The steady-state solution yields an explicit formula for the γ value as

$$\gamma = 3\frac{\alpha_{vis} - \alpha_{uv}(\alpha_{uv} + (1-\alpha_{vis})e^{n_{uv}}) + (1+\alpha_{uv})(\alpha_{uv} - \alpha_{vis})e^{n_{uv}}e^{n_{vis}}}{\alpha_{vis} - 2\alpha_{uv}(1+\alpha_{uv}+\alpha_{vis}) + 3\alpha_{uv}\alpha_{vis}e^{n_{uv}} + (1+\alpha_{uv})(2\alpha_{uv} - \alpha_{vis})e^{n_{uv}}e^{n_{vis}}} \quad (7)$$

For consistence check, Eq. 7 satisfies the condition of $\gamma = 0$ at $\alpha_{uv} = 1$ and $\alpha_{vis} = 1$ (zero bias for leg displacement). The numerator and denominator both become zero at $n_{uv} = 0$ and $n_{vis} = 0$, which corresponds to the trivial limit of no light operation. For large n_{uv} and n_{vis} corresponding to effective light operation, Eq. 7 clearly yields the $\gamma = 1.5$ limit: both the numerator and denominator can be approximated by the terms with $\exp(n_{uv})$ $\exp(n_{vis})$, leading to $\gamma \approx \frac{3}{2}\left(1 - \frac{\alpha_{vis}}{2\alpha_{uv} - \alpha_{vis}}\right) < 1.5$ for plus-end-directed biases or no bias (i.e., $\alpha_{uv} \geq 1$ and $\alpha_{vis} \leq 1$).

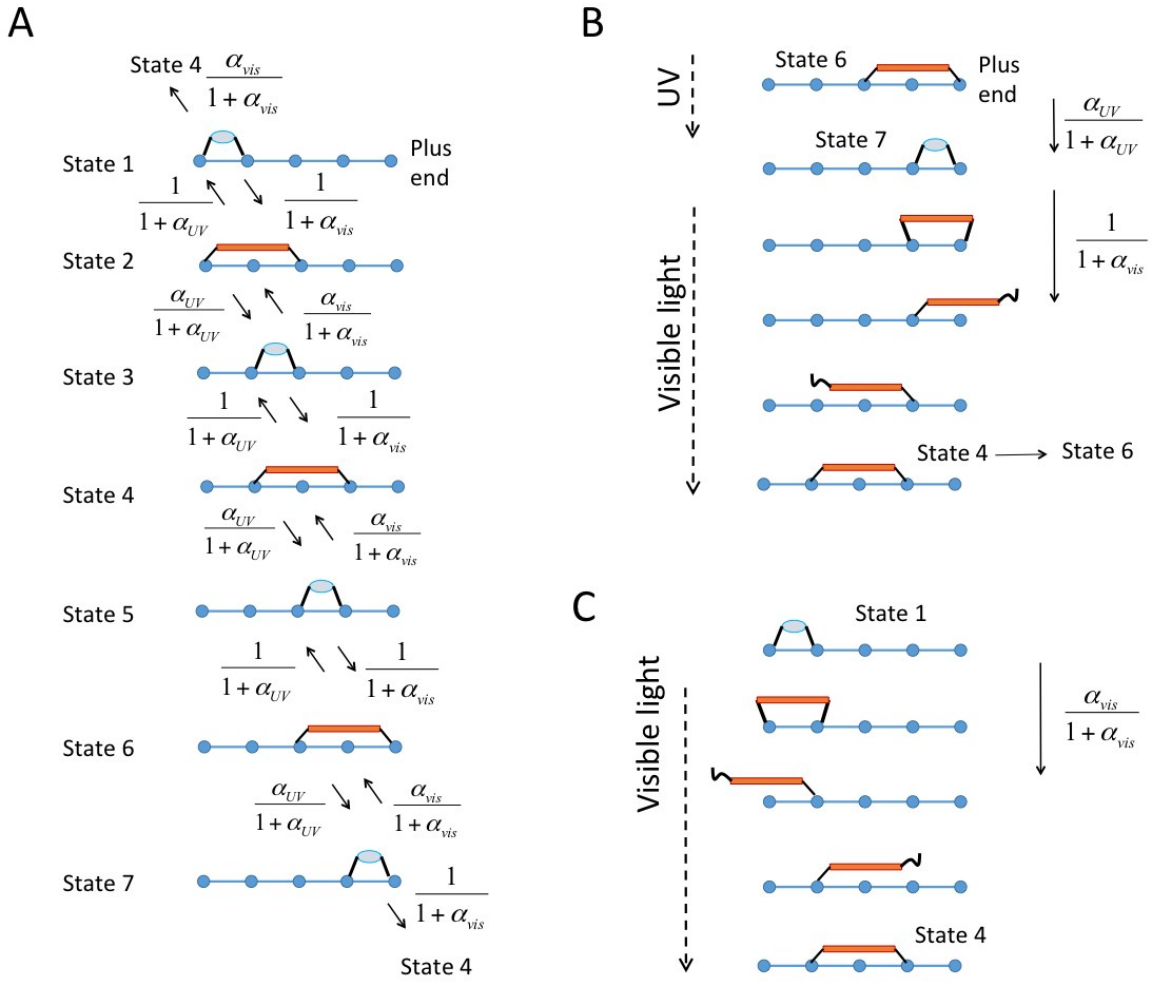

Figure S2. The kinetic model for an inchworm walker operating on a 5-site track. A. All possible two-leg-bound states of the motor, which match two nearest binding sites (solid sphere) in a contracted configuration and match three sites in an extended configuration. The light-induced transitions between these states are indicated (arrows), for UV and visible light, respectively. The branch ratio for the transitions from each state is shown (subscripts 'uv' and 'vis' for UV and visible light, respectively). A branch ratio of $\alpha_{uv} > 1$ indicates a preference for forward displacement of the trailing leg versus backward displacement of the leading leg in the UV-induced stroke, and $\alpha_{uv} < 1$ indicates a preference for forward displacement of the leading leg versus backward displacement of the trailing leg. B. Schematic illustration of the flip-flop pathway for the visible light-induced transition from a contracted motor at the track's plus end (state 7 in panel A) to an extended motor in the middle of the track (state 4). The plus-end-directed inchworm motion once again sends the walker from state 4 back to state 7 through state 6, resulting in a cycling of the walker at the plus end. C. A similar flip-flop pathway for the transition to state 4 from the contracted motor state at the track's minus end (state 1).

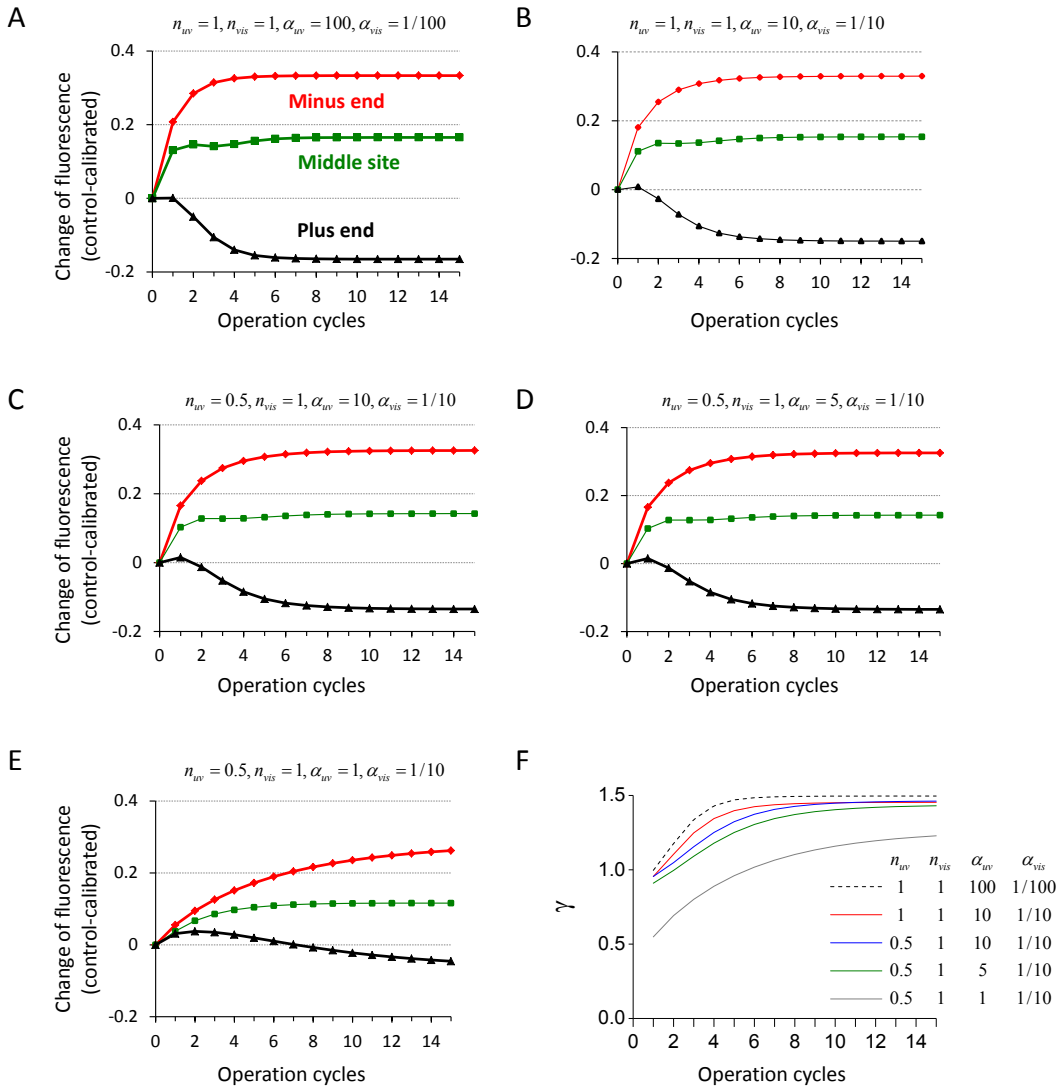

Figure S3. The predicted control-calibrated fluorescence and γ values versus the number of operation cycles (each cycle consists of UV plus visible light). The results are obtained from the time-dependent solution of the kinetic model (eq. 5). The dashed line in panel F (also shown in Fig. 2 E–H) corresponds to near perfect inchworm motion (100% effectiveness for light-induced leg displacement, i.e., $n_{uv} = 1$, $n_{vis} = 1$; and 100:1 ratio for forward over backward displacement, i.e., $\alpha_{uv} = 100$, $\alpha_{vis} = 1/100$). The solid lines show γ for reduced effectiveness and biases, which are more relevant to the present DNA walker. Note that $n_{vis} \sim 1$ is realistic due to the very effective[2, 3] cis-to-trans switch of DNA-embedded azo-moieties by visible light. Panels A – F show the predictions at different effectiveness/bias for the UV-induced stroke. Similar results are obtained by changing effectiveness/bias for the visible light-induced stroke. The predicted fluorescence change shows a pattern of rising and saturating minus-end signal but less drop of plus-end signal, which is similar to the data of the DNA walker (Fig. 2). The magnitude of fluorescence change of the real walker is reduced as compared to the predictions since the predictions are for ideal walkers.

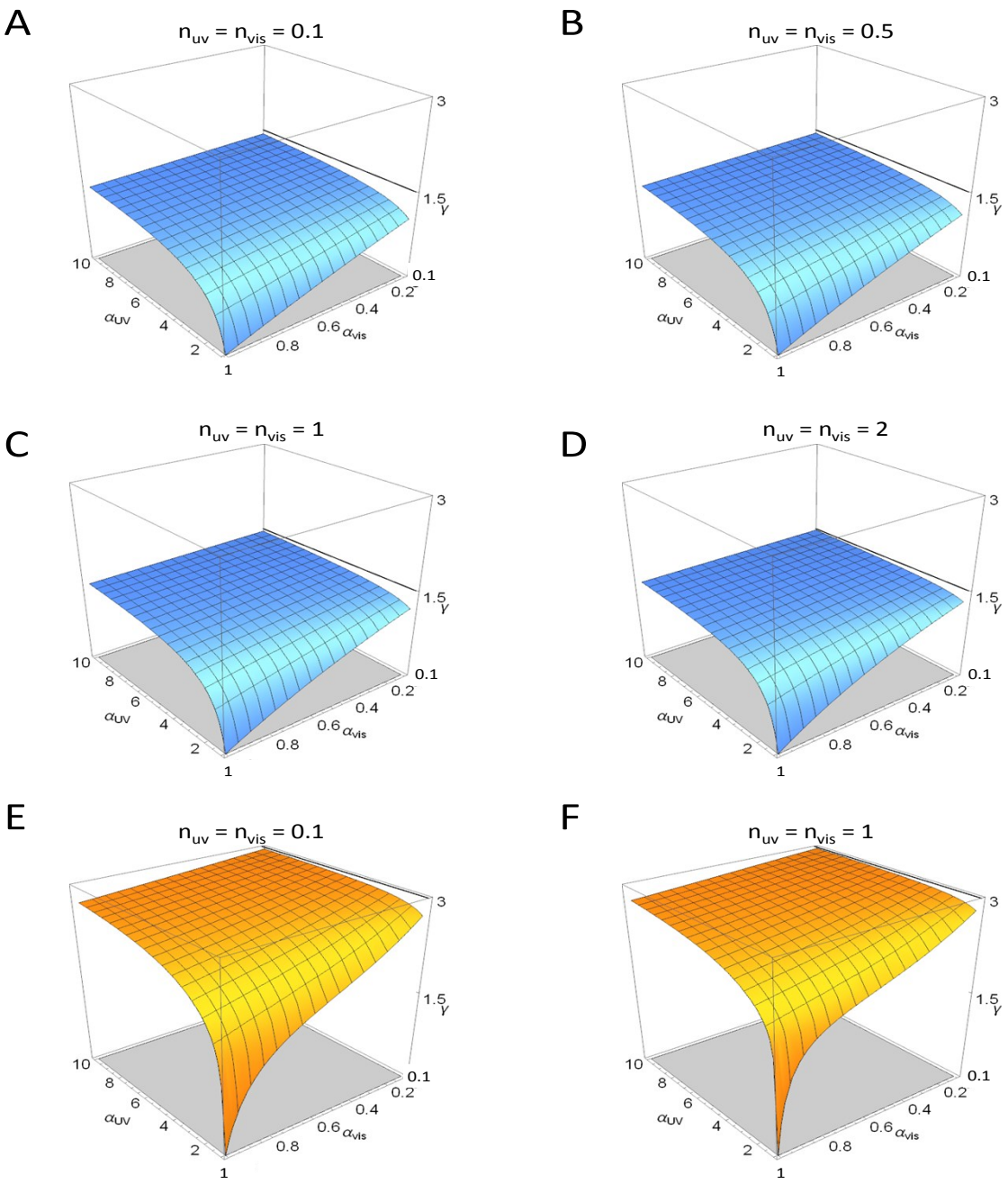

Figure S4. The γ values from steady-state solution of the kinetic model (eq. 7), which corresponds to the walker's asymptotic performance after many rounds of UV-visible light operation. Shown are the γ values obtained by exhaustively scanning the four parameters of the kinetic model. Panels A – D are the prediction from the full transition diagram (Figure S2, panel A). Panels E, F are the prediction ignoring the flip-flop transitions from the track's ends (Figure S2, panels B, C).

3. Extra data

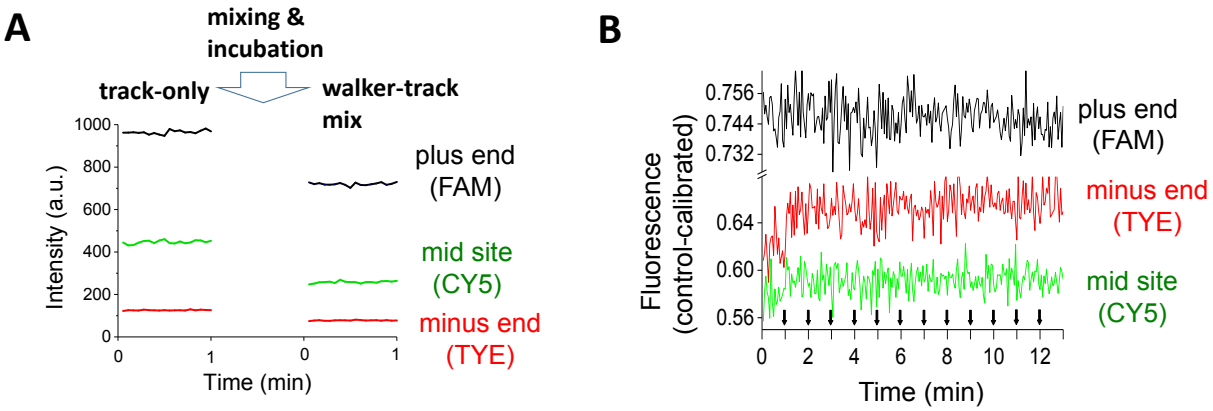

Figure S5. Panel A. The fluorescence intensity from the three dyes of a 5-site track before and after equimolar mixing with the walker and a long incubation (18 hours). Panel B. The control-calibrated fluorescence for the walker operated on the 5-site track under 20m UV/1m visible light. The time shown covers only the rounds of visible light, during which fluorescence data are recorded. The arrows indicate the time when the UV is applied. The data shown here yield the fluorescence change shown in Fig. 2A.

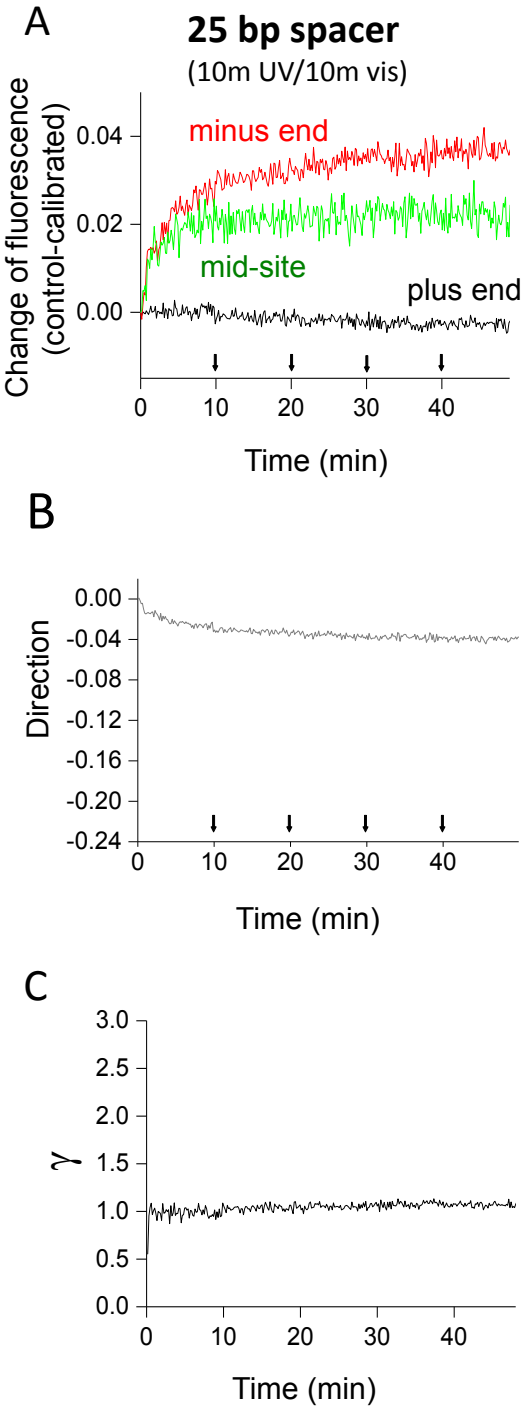

Figure S6. Performance of the walker on the 5-site track (imperfect 25bp spacer) under operation of 10m UV/10m visible light (arrows indicate the time when the UV is applied). The data are collected and analyzed by the same procedure as for Fig. 2 except for different UV/visible light durations.

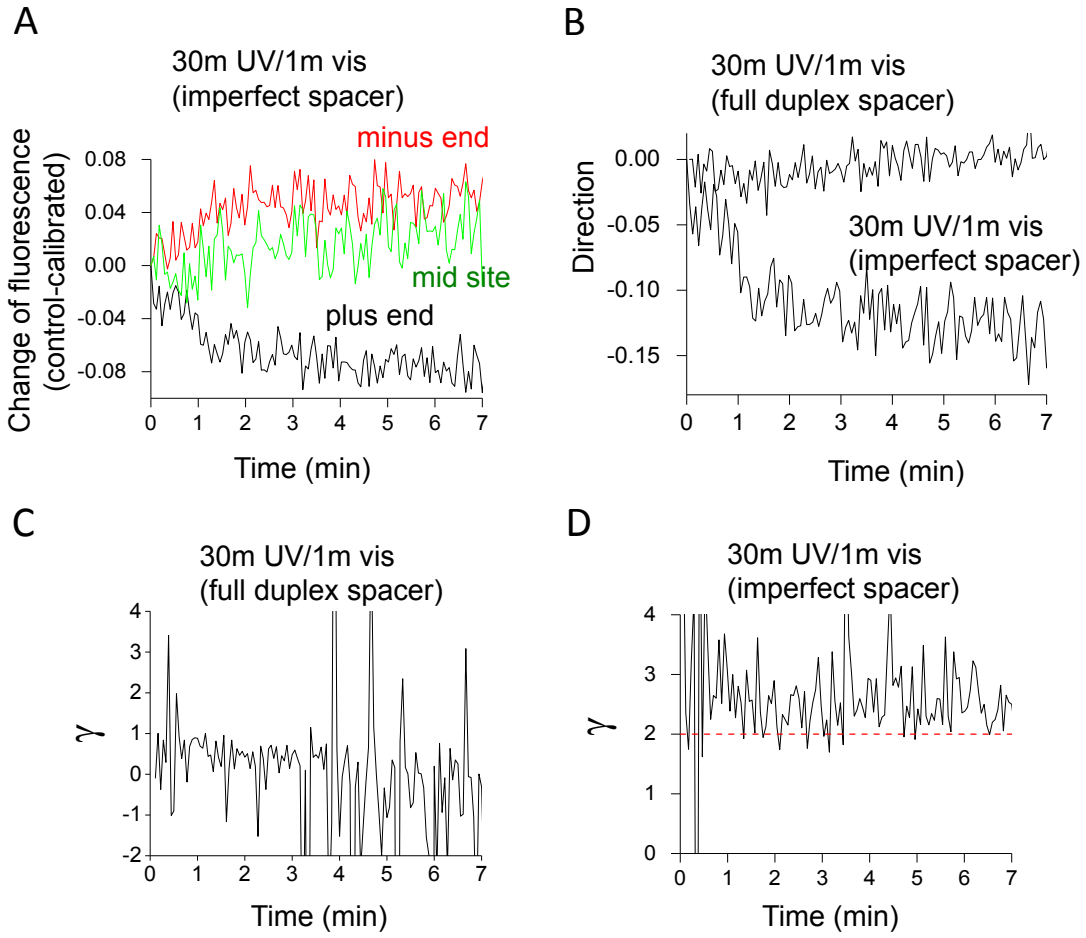

Figure S7. Fluorescence signals (panel A), direction signal (panel B), and γ values (panels C, D) for the walker on the 5-site track with 25bp spacer under operation of 30m UV/1m visible light. The experimental procedures are the same as for Fig. 2 except for different UV durations.

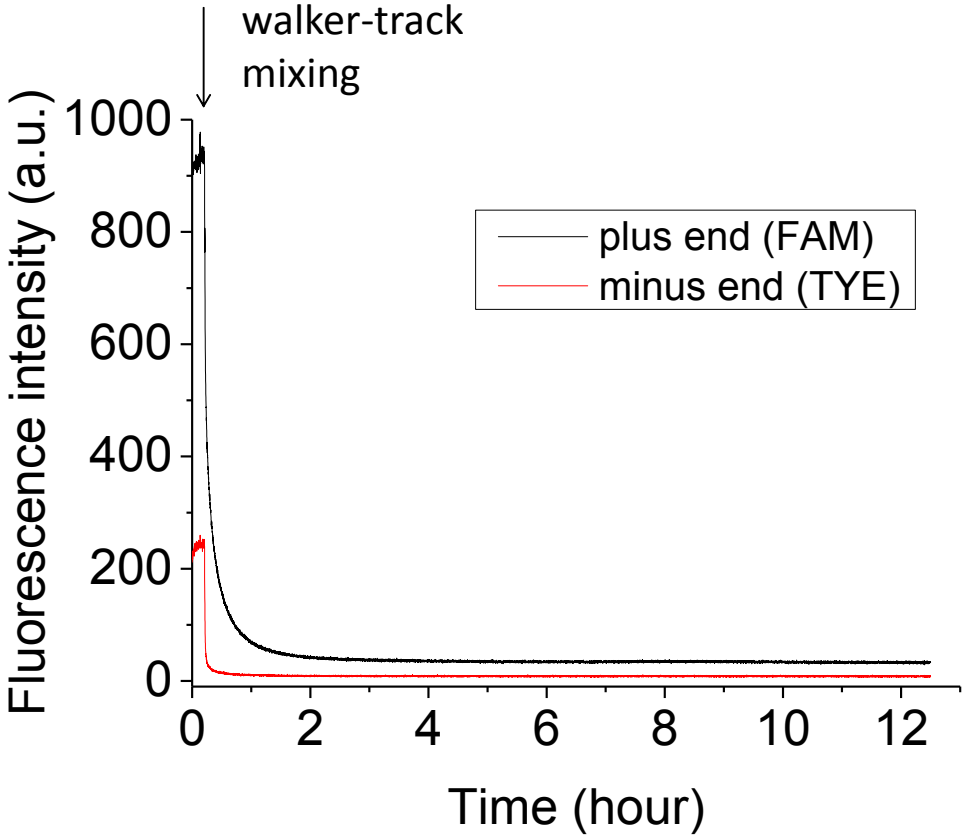

Figure S8. The binding experiment preparing the walker-track complex for the bias experiment shown in Fig. 3A. The mixing is started at the time as indicated (equimolar). The early drop of fluorescence intensity indicates walker-track binding. The intensity for either dye becomes flat over 4 – 12 hours, indicating negligible photobleaching.

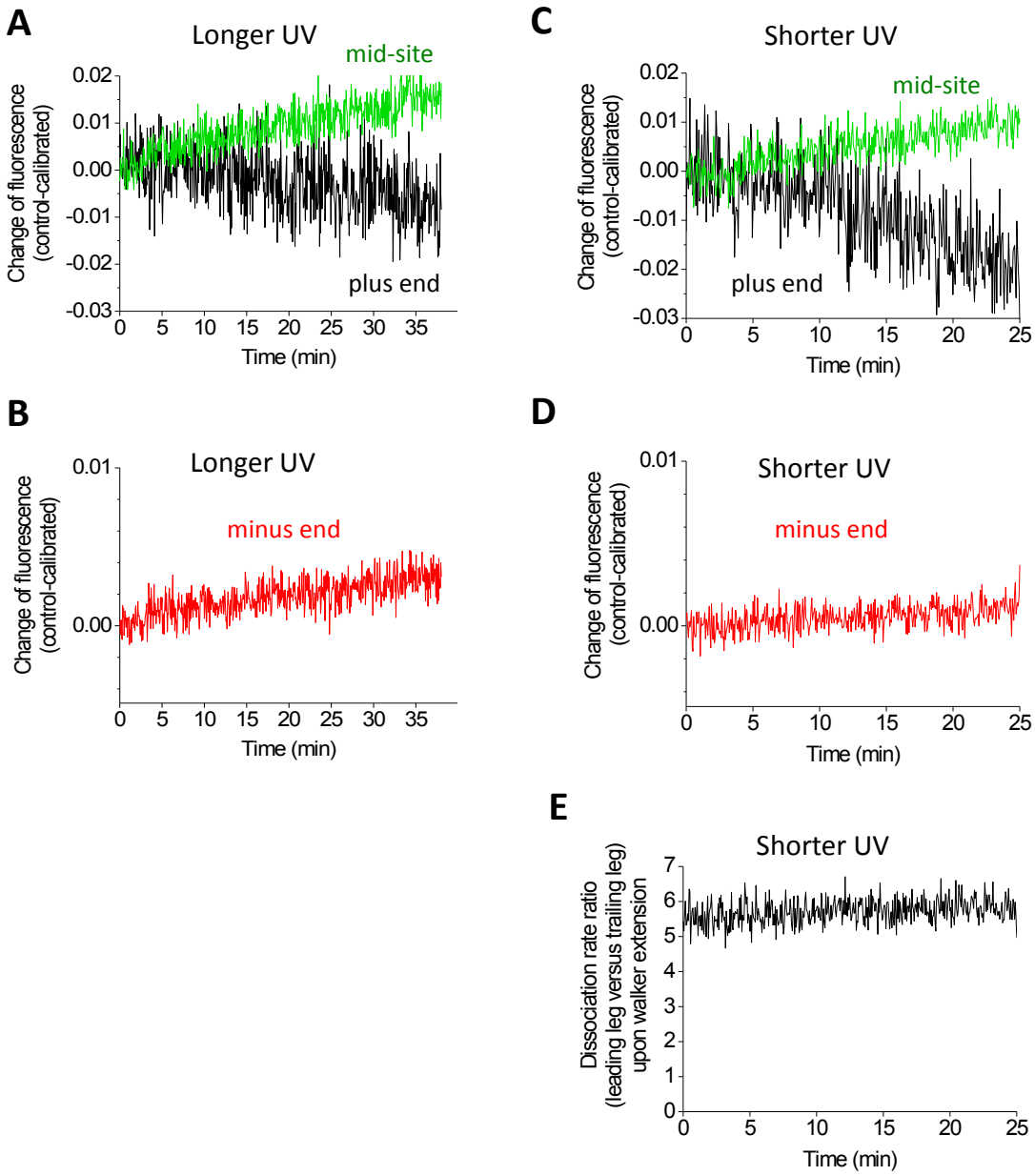

Figure S9. Change of fluorescence signals extracted from the operation experiment shown in Fig. 4 (panels A, B) and from a new experiment by the same procedure but with a shorter UV duration (panels C, D). In the new experiment, the UV light lasts 30 minutes each and is applied at 1, 2, 3, …, 24 minute along the time axis (only visible light duration shown during which the fluorescence data are collected). Panel E shows the dissociation rate ratio extracted from the data in panels C, D.

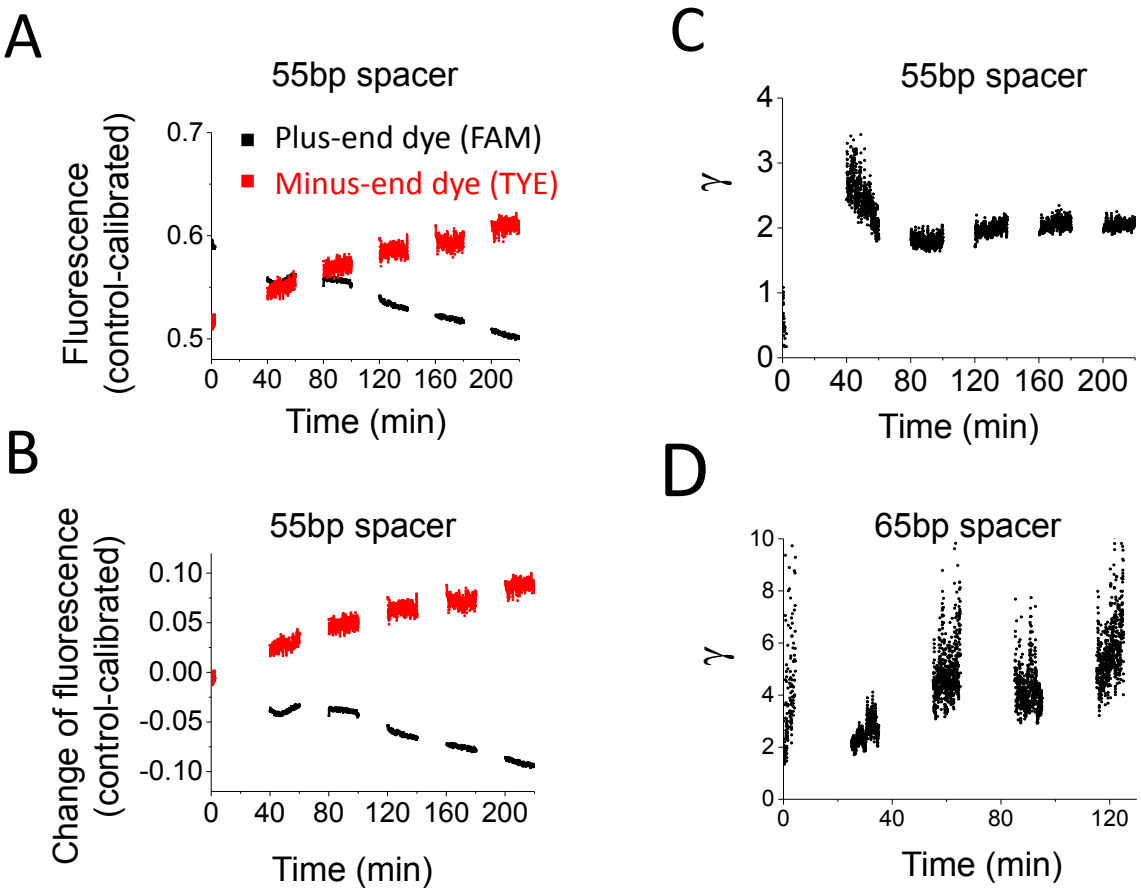

Figure S10. Performance of the walker operated on a truncated 3-site track with a 55bp spacer (see the track design in Figure S1, panel D). The shown data span the visible light time while the gaps are the UV time. The fluorescence data in panels A, B yield one set of direction signals shown in Fig. 4D. The data are collected and analyzed by the experimental procedure as for Fig. 2 except for the use of 3-site track and a lower motor-track concentration (5nM).

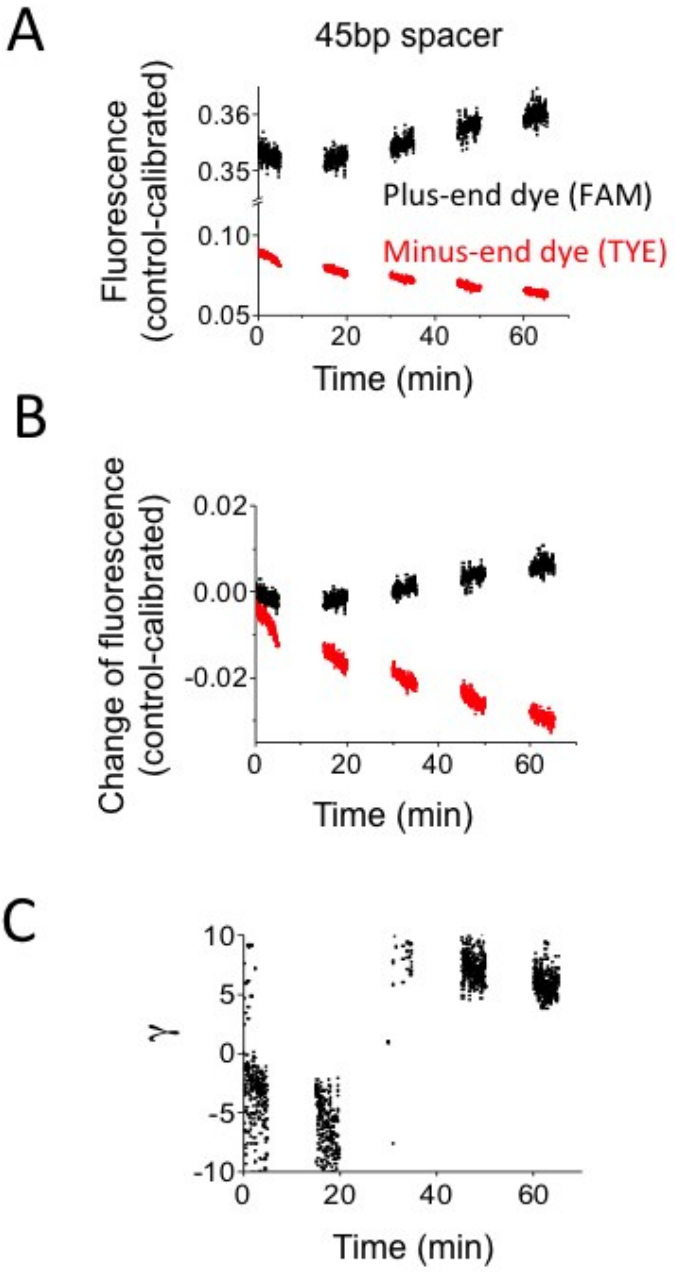

Figure S11. Performance of the walker operated on a truncated 3-site track with a 45bp spacer. The shown data span the visible light time while the gaps are the UV time. The fluorescence data in panels A, B yield one set of direction signals shown in Fig. 4D. The fluorescence data are collected and analyzed by the experimental procedure as for Fig. 2 except for the use of 3-site tracks and a lower motor-track concentration (5nM). Since the walker shows a minus-end-directed motion, the γ data in panel C are now extracted from the fluorescence data as the change of control-calibrated fluorescence from the plus end (black in panel A, B) minus that from the minus end (red) and then divided by the plus-end signal.

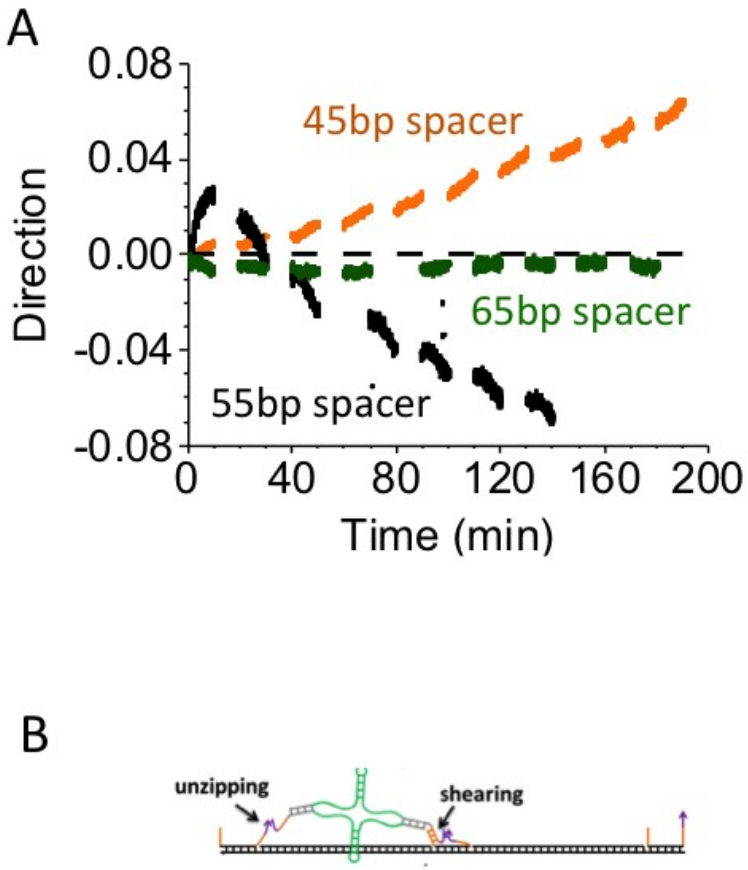

Figure S12. A. Direction of a previously reported bipedal DNA walker operating on the same truncated 3-site track with different inter-site spacers as shown in Figure S1 (panel D). This walker is also operated by alternating UV and visible light. The data span the visible light time while the gaps are the UV time (all data collected at a motor-track concentration of 5 nM). The direction signals shown are extracted from the control-calibrated fluorescence by the same procedure as for Fig. 6A–D. B. Schematic illustration of the walker. It has the same legs as the present one but an azo-embedded double-hairpin engine that extends under UV and contracts under the visible light. More details of the walker can be found in ref.[4].

References

1. P. Alberti and J. Mergny, *Proc. Natl. Acad. Sci. USA*, 2003, **100**, 1569-1573.
2. X. Liang, T. Mochizuki and H. Asanuma, *Small*, 2009, **5**, 1761-1768.
3. J. Cheng, S. Sreelatha, R. Z. Hou, A. Efremov, R. C. Liu, J. R. van der Maarel and Z. S. Wang, *Phys. Rev. Lett.*, 2012, **109**, 238104.
4. I. Y. Loh, J. Cheng, S. R. Tee, A. Efremov and Z. S. Wang, *ACS Nano*, 2014, **8**, 10293-10304.